High Voltage

Special Issue: Selected Papers from the 2018 IEEE International Conference on High Voltage Engineering and Application (ICHVE 2018)

IET Journals
The Institution of Engineering and Technology

High voltage outdoor insulator surface condition evaluation using aerial insulator images

eISSN 2397-7264
Received on 30th March 2019
Revised 31st July 2019
Accepted on 1st August 2019
E-First on 12th September 2019
doi: 10.1049/hve.2019.0079
www.ietdl.org

Damira Pernebayeva[1], Aidana Irmanova[1], Diana Sadykova[1], Mehdi Bagheri[1], Alex James[1] ✉

[1]*Department of Electrical and Computer Engineering, School of Engineering and Digital Sciences Nazarbayev University, Astana, Kazakhstan*
✉ *E-mail: apj@ieee.org*

Abstract: High voltage insulator detection and monitoring via drone-based aerial images is a cost-effective alternative in extreme winter conditions and complex terrains. The authors examine different surface conditions of the outdoor electrical insulator that generally occur under winter condition using image processing techniques and state-of-the-art classification methods. Two different types of classification approaches are compared: one method is based on neural networks (e.g. CNN, InceptionV3, MobileNet, VGG16, and ResNet50) and the other method is based on traditional machine learning classifiers (e.g. Bayes Net, Decision Tree, Lazy, Rules, and Meta classifiers). They are evaluated to discriminate the images of insulator surface exposed to freezing, wet, and snowing conditions. The results indicate that traditional machine learning methods with proper selection of features can show high classification accuracy. The classification of the insulator surfaces will assist in determining the insulator conditions, and take preventive measures for its protection.

1 Introduction

Outdoor electrical insulators are critical components in high voltage power transmission and distribution lines. The insulators are deployed to provide the mechanical support and electrical isolation to conductors. The in-service insulators operating under severe environment are affected by several significant factors such as weathering and airborne contamination.

The outdoor insulators are prone to mechanical and electrical stresses that deteriorate dielectric property leading to their failures. Leakage current in the insulators is indicative of the failures. The increase in contamination from airborne pollution such as soluble deposits (sea-salt, industrial oil, and dust, ice) are known to cause degradation [1]. The contamination of the insulator surface also contributes to a decrease in the creepage distance, causing flashover, and can even decrease the insulator's puncture voltage level. There are other factors such as vandalism [2], inclement weather conditions [3, 4], aging [5], erosion, and tracking [6] that can cause the failures in the insulation system.

The extreme weather conditions, such as, that lead to ice and snow formation on insulator surfaces in combination with wind conditions can cause additional mechanical load that leads to the reduction of the leakage distance of insulators [7]. The wet-conditions of the surface along with the non-uniformly polluted surface creates a distortion of the electric field forming a conductive layer that decreases surface resistance, triggers surface discharge [8] and leakage current [9–11]. This makes condition monitoring and evaluation of insulators state important for power utilities. Condition assessment of insulator aims to identify the current condition of energised insulators and take remedial actions if required by replacing faulty insulators.

Conventional monitoring approaches for high voltage overhead insulators becomes challenging task under several situations such as (i) changes in weather conditions, (ii) geographically isolated locations and terrains, (iii) the cost factors such as for experts and measurement setups, and (iv) by the sheer volume of insulators to be analysed. Traditional insulator monitoring techniques rely on visual inspection via ground patrolling, pole climbing, and aerial inspection using a helicopter and different cameras, including thermal-infrared or ultrasound cameras. A ground patrolling method can provide an accurate defect detection rate; however, this method is labour-intensive and affected by weather conditions. Whereas, aerial inspection by manned helicopter can cover the large size of the power network, but limits detection accuracy due to flight speed and considerable distance to power line objects. These traditional approaches are costly, time-consuming, and are efficient and cost-effective due to the large size of the transmission networks and complex geographic locations.

The real-time and continuous condition monitoring system for power line infrastructure including outdoor electrical insulators using image processing and unnamed aerial vehicles (UAVs) is growing popularity due to the possibility to automate the condition monitoring at low cost and can be an alternative to ground-based systems and helicopters. With UAVs, it is possible to fly closer and collect real-time spatial data using infrared, thermal, and optical sensors by hovering over electrical transmission insulators. The UAV operation includes data acquisition, the transmission of information to the on-site control station for UAV navigation, recording the location of investigated equipment, and information transmission to the base station for image data analysis. Several studies have focused on this topic by introducing various image processing algorithms to detect the insulators in aerial images and its fault diagnosis [12, 13].

In this work, we examine the condition of outdoor glass insulators exposed to freezing winter condition and pollution. The aerial images done for this study is obtained from drones under extreme winter weather conditions typical of the Eurasian region. We extend our previous work in [14] by including further analysis with data-driven neural network classifiers such as convolutional neural networks, to draw a comparison with traditional machine learning (ML)-based approaches. The primary objective in this work is to identify and discriminate the presence of the ice, water, and snow formation over the insulator surface, analysing the aerial images of the insulator.

We examine and compare the performance of the neural network and ML classification algorithms using insulator image data set. For the traditional ML classifiers, the impact of using feature extraction and normalisation is analysed. The deep learning methods are compared for performance on different networks. The main contributions of this work are as follows: (i) this work shows that traditional ML algorithms can be equally competitive to that of deep learning approaches, (ii) the need for optimisation of deep learning approaches for the given classification problem is

a *b* *c* *d*

Fig. 1 *Glass insulator images*
(a) Clean, ***(b)*** Water, ***(c)*** Snow, ***(d)*** Ice

a *b* *c*

Fig. 2 *Images samples of clean insulator surface processed by filters*
(a) Retinex, ***(b)*** LMN, ***(c)*** Mean

a *b* *c*

Fig. 3 *Images samples of snow-covered insulator surface processed by filters*
(a) Retinex, ***(b)*** LMN, ***(c)*** Mean

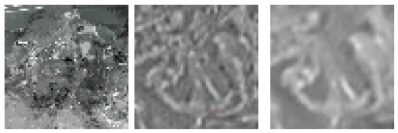

a *b* *c*

Fig. 4 *Images samples of ice-covered insulator surface processed by filters*
(a) Retinex, ***(b)*** LMN, ***(c)*** Mean

a *b* *c*

Fig. 5 *Images samples of water droplets on insulator surface processed by filters*
(a) Retinex, ***(b)*** LMN, ***(c)*** Mean

highlighted rather than using the pre-trained neural network models.

The paper is organised into five main sections with Section 2 providing details of image acquisition using a drone, image normalisation using filters: retinex, mean and local mean normalisation (LMN), and feature extraction using standard deviation (STD) and local binary patterns (LBPs) descriptors. Section 3 provides the details of the classification using Bayes Naive, Bayes Net (BN), IBK, sequential minimal optimisation (SMO), J48, Random Forest (RF) and AdaBoost (AB) M, and convolutional neural networks. Section 4 provides a summary of results and discussions, with Section 5 drawing the main conclusions of the paper.

2 Image processing

2.1 Image acquisition

The image data set consists of aerial images of a suspended glass insulator captured using a drone at different view angles and dynamic conditions. The insulator was hung outside during the wintertime and the images of ice and snow formation, as well as a wet condition over the surface were captured periodically using a drone DJI Phantom 4. The data set contained 400 images with four classes, including snow, water, ice, and clean surface with 100 images in each class. The size of the original images was scaled down and segmented by 64×64 pixel size to reduce the computational cost. The original images of high voltage glass insulator under different weather condition are given in Fig. 1.

2.2 Image filtering

The aerial images acquired in dynamic mode usually have extreme variations in the intensity of illumination, making it challenging to capture informative images with traditional onboard cameras in drones. Therefore, image filtering techniques such as Retinex filter, LMN and mean filters are applied to reduce the noise, non-uniform illumination effects, and enhance the images. The filters used for creating the data set in our study was implemented in MATLAB. The images of four conditions of insulator surface processed by these filters are presented in Figs. 2–5.

2.2.1 Retinex filter: The retinex-based algorithm is a widely used tool to enhance and restore images by preserving object details. The retinex theory was first proposed by McCann [15], and it states that the scene in the human eye is the product of reflectance (R) and illumination (L) as shown in (1). Here, illumination refers to the presence of light falling on the object when the image is taken, and reflectance is the intensity of light reflected by the object. Generally, the filter utilises local mean of pixels whose values are higher than the centre to calculate illumination, however, noise in the sense of halo artefacts may appear near the reflectance edges, which results in unnatural detail retrieval [16]. The input images were processed in MATLAB by setting the parameters of the filter.

$$I(x, y) = L(x, y)R(x, y) \tag{1}$$

2.2.2 LMN filter: The influence of image illumination on classification results tends to be very high. The simple and effective solution to this issue could be the implementation of normalisation by local standardisation of feature vectors [17]. The normalised feature vector is characterised by (2). The output $y(i,j)$ is obtained using the original image, which is defined as $I(i,j)$ with local mean $\overline{I_g}(i, j)$ and STD estimated by Gaussian kernel with $\sigma_g(i, j)$. The function is implemented in MATLAB by setting the smoothing windows $\sigma_g(i, j)$.

$$y(i, j) = \frac{I(i, j) - \overline{I_g}(i, j)}{\sigma_g(i, j)} \tag{2}$$

2.2.3 Mean filter: The mean filter is considered to be the simplest form of denoising filter as it is efficient and simple in terms of performance and cost. The image signal is processed by averaging values of neighbourhood pixel intensities for fixed window size. Basically, the filtering process involves convolution of an input image and the filter mask (kernel) with 2×2 size. This filter is applied to compare the influence of object smoothing on classification performance.

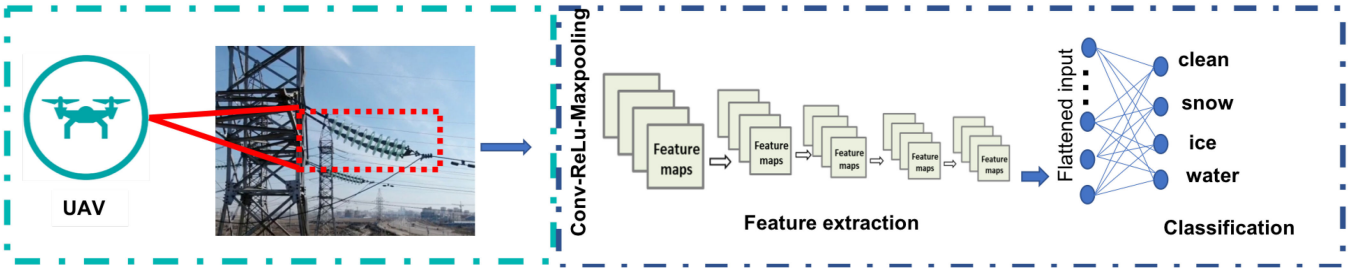

Fig. 6 *Proposed CNN architecture for UAV acquired images*

2.3 Feature extraction

Two different feature extraction approaches – LBP filtering and mean-variance filtering were examined to transform images to feature vectors. The LBP is a simple but effective texture descriptor widely used in applications requiring illumination invariant features [18]. In our experiment, LBP is chosen for texture feature extraction due to its benefits such as computational efficiency and invariance to greyscale changes. To describe the texture information in the images LBP assigns a label to every pixel of an image by thresholding the 3×3 – neighbourhood of each pixel with the centre pixel value and considering the result as a binary number as described through (3) and (4) [19]

$$\mathrm{LBP_P} = \sum_{p=0}^{P-1} s(g_\mathrm{p} - g_\mathrm{s}) 2^p \tag{3}$$

$$s(x) = \begin{cases} 1, & \text{if} \quad x \geq 0 \\ 0, & \text{otherwise} \end{cases}, \tag{4}$$

Here, p is the index of the pixel in the neighbourhood of the pixel g_s. $s(x)$ thresholds the distance between the neighbourhood pixels to binary relative to the g_s pixel. The mean-variance filtering is a feature representation that standardises the pixel range within a local window. The filter substitutes the original pixel-value with a STD window mask in an area around the pixel. This operation resembles the human eye sensory filtering process resulting in edges of different strengths determined by the window size.

3 Classification

3.1 ML algorithms

The classification algorithms are tested on the database containing four classes of the surface condition of outdoor high voltage glass insulator (clean, water, ice, and snow) and 100 images within each class. The images are pre-processed by LMN, retinex filters, and mean filters to make the feature illumination invariant. The feature vectors formed using LBP and STD descriptors are used in different classifiers for recognition accuracy tests. Two metrics used for performance evaluation of classifiers: area under the receiver operator characteristic curve [area under the curve (AUC)] and accuracy (%). We select the following classifiers: J48, Bayes Naive, BN, IBK, SMO, RF, and Ada Boost M1.

3.1.1 BN and Naive Bayes (NB): BN and NB are widely used techniques that belong to the group of Bayesian network classifier and operate as probabilistic graph models. To compute the conditional probability of each attribute, assuming that it is as statistically independent, for the given class by learning from training data, and then predict the class with the highest posterior probability [20]. The Bayes classifier is a probabilistic function that assigns a class label $\hat{y} = C_k$ for some k as follows: $\hat{y} = \underset{k \in \{1, \ldots, K\}}{\operatorname{argmax}} \; p(C_k) \prod_{i=1}^{n} p(x_i | C_k)$.

3.1.2 SMO: SMO classifier is one of the functional classifiers, which operates similar to the neural network. The SMO is designed to resolve the problems arising in support vector machine (SVM) and utilised for training the SVM using polynomial or radial basis function (RBF) kernels by replacing the missing values and converting nominal attributes into binary ones [21, 22].

3.1.3 IBK: IBK is also known as K-nearest neighbour and is included under the category of Lazy classifiers. This type of classifier is simple and effective in operation. However, it is memory intensive and time-consuming since it stores training instances and does not support the inclusion of new samples in training set while building the model.

3.1.4 J48 andRF: Decision tree J48 and RF are well-known classification algorithms, which use a tree structure, which is formed from a set of labelled training data. Each node in the tree model denotes a test on the attribute value and the outcome of every test is represented by each branch. In IBK model, the tree leaves represent the predicted classes, and the decision is made by splitting the data into smaller subsets using each attribute, whereas the RF produces the output in the form of individual trees [23].

3.1.5 AdaBoost M1: AB M1 is Meta type classifier, which is used to generate and train a base classifier through determining the optimal set of attributes. It helps to reduce the learning error and improve the prediction performance of the base classifier [24].

3.2 CNN

The convolutional neural network is a representative model of deep learning. It is a powerful tool widely implemented for image-related analysis. The advantages of the implementation of CNN are due to its sparse connection, parameter reduction through weight sharing, a high degree of invariance for translation, scaling, and tilting [25, 26]. The CNN-based approach has proven to be feasible to train large data set in visual recognition problems for different application domains, including insulator detection [27, 28] and diagnosis [29]. The CNN operates to extract mid-level and high-level features from input images by shrinking the feature maps.

3.2.1 Feature extraction: In the input layer, the greyscale image with the size of $64 \times 64 \times 1$ is fed as an input, then multiple convolutional and sub-sampling or pooling layers are utilised to extract the feature characteristics by implementing partial sub-sampling and local averaging. The convolutional layer simply computes the feature map of an input image by applying and sliding a trainable filter bank with a certain size of $1 \times 1 \times k$ (k-number of channels, same as an input image) around the image. The convolution is a repeatable matrix multiplication of the pixel values of the input image with the values in the filter for every location on the input image. In our network, five convolutional layers with $32 \times 3 \times 3$ are used to create feature maps. The rectified linear unit (ReLu) as activation function is chosen to introduce non-linearity into convolution network. ReLu is a simple and fast computing function that operates by thresholding values at 0, $f(x) = \max(0, x)$. The pooling layer is introduced to reduce computational complexity by downsampling the feature map and decreasing the size of parameters. It extracts sub-regions of the feature map, keeps their maximum value, and discards all other values, and this helps to avoid overfitting. After extracting and learning the features, all features are flattened and transformed into one feature vector and fed to a fully connected layer. The CNN architecture is illustrated in Fig. 6.

Table 1 Performance of ML classifiers: clean insulator surface

Measure	Processing	BN	NB	SMO	IBK	AdaBoostM1	J48	RF
accuracy, %	STD/mean	79.35(4.79)	75.00(0)*	75.00(0)*	74.83(6.08)*	75.88(3.42)	77.67(5.25)	76.70(5.74)
AUC	STD/mean	0.76(0.07)	0.78(0.08)	0.50(0.00)*	0.66(0.07)*	0.79(0.07)	0.76(0.08)	0.80(0.07)
percent correct	STD/LMN	**91.50(3.86)**	74.35(1.21)*	75.00(0.00)*	91.07(4.18)	**91.60(3.93)**	90.93(3.85)	**90.70(4.69)**
AUC	STD/LMN	**0.92(0.05)**	0.70(0.08)*	0.50(0.00)*	0.88(0.06)*	**0.92(0.04)**	0.90(0.06)	**0.95(0.04) v**
accuracy, %	STD/Retinex	74.83(1.79)	73.85(3.25)	75.00(0.00)	73.93(5.96)	77.65(3.37) v	77.95(4.89)	78.05(5.62)
AUC	STD /Retinex	0.59(0.05)	0.65(0.11)	0.50(0.00)*	0.64(0.08)	0.70(0.09) v	0.69(0.08) v	0.73(0.10) v
accuracy, %	LBP/mean	77.60(5.33)	77.18(5.36)	67.78(6.41)*	76.87(2.60)	71.85(6.02)*	70.30(5.86)*	75.88(1.48)
AUC	LBP/mean	0.64(0.08)	0.86(0.05)	0.74(0.06)	0.55(0.05)*	0.67(0.08)	0.61(0.09)	0.81(0.06)
accuracy, %	LBP/LMN	77.70(4.05)	67.85(6.50)*	76.72(4.55)	75.00(0.71)	70.20(5.05)*	66.63(7.24)*	75.00(0.00)
AUC	LBP/LMN	0.59(0.07)	0.65(0.09)	0.77(0.08)	0.50(0.01)	0.56(0.11)	0.55(0.11)	0.58(0.12)
accuracy, %	LBP/Retinex	78.42(5.35)	72.98(6.25)*	67.98(7.39)*	80.30(3.96)	71.02(5.34)*	70.63(6.19)*	78.50(2.93)
AUC	LBP/Retinex	0.62(0.08)	0.69(0.09) v	0.66(0.09)	0.61(0.08)	0.61(0.11)	0.62(0.10)	0.74(0.11) v

The bold values represent the best classification accuracy metrics of machine learning algorithms in "%" and "AUC" metrics.

Table 2 Performance of classifiers: ice on insulator surface

Measure	Processing	BN	NB	SMO	IBK	AdaBoostM1	J48	RF
accuracy, %	STD/mean	79.65(6.60)	80.73(5.46)	74.73(0.93)*	74.97(5.53)*	79.07(6.55)	78.82(6.50)	7 8.60(5.76)
AUC	STD/mean	0.85(0.05)	0.89(0.05) v	0.50(0.01)*	0.66(0.07)*	0.86(0.05)	0.83(0.06)	0.86(0.05)
accuracy, %	STD/LMN	85.83(4.57)	56.98(7.56)*	75.00(0.00)*	81.58(6.07)*	75.00(0.00)*	85.80(4.82)	84.30(4.91)
AUC	STD/LMN	0.87(0.06)	0.69(0.09)*	0.50(0.00)*	0.76(0.08)*	0.69(0.04)*	0.87(0.06)	0.89(0.06)
accuracy, %	STD/Retinex	75.00(0.00)	73.27(5.55)	75.00(0.00)	73.03(6.46)	75.00(0.00)	75.00(0.00)	76.73(6.29)
AUC	STD /Retinex	0.71(0.07)	0.75(0.08) v	0.50(0.00)*	0.64(0.09)*	0.70(0.06)	0.50(0.00)*	0.78(0.08) v
accuracy, %	LBP/mean	**96.25(2.69)**	**94.82(2.94)**	90.68(4.26)*	67.70(6.29)*	78.30(5.84)*	73.43(6.97)*	79.10(2.90)*
AUC	LBP/Mean	**0.97(0.03)**	**0.99(0.01)v**	0.88(0.07)*	0.59(0.11)*	0.81(0.07)*	0.63(0.10)*	0.99(0.01) v
accuracy, %	LBP/LMN	79.40(3.66)	69.73(4.99)*	75.37(2.02)*	73.25(2.42)*	71.50(5.01)*	67.32(6.91)*	75.00(0.00)*
AUC	LBP/LMN	0.60(0.07)	0.63(0.07)	0.58(0.06)	0.49(0.02)*	0.57(0.10)	0.58(0.10)	0.64(0.11)
accuracy, %	LBP/Retinex	79.63(4.01)	76.78(5.61)	66.00(7.04)*	76.60(3.84)	73.13(5.32)*	68.78(6.26)*	77.60(5.06)
AUC	LBP/Retinex	0.62(0.06)	0.78(0.07) v	0.73(0.07) v	0.58(0.06)*	0.67(0.10)	0.61(0.09)	0.72(0.09) v

3.2.2 Classification: The fully connected neural network, also known as a densely connected network, perform the inference for classification. The last layer of this network is a softmax operator that indicates the probability of the class. The structure of the network is feed-forward and uses the back-propagation algorithm for learning. A feed-forward model computes the output based on the given input data, whereas the back-propagation learning algorithm adjusts the weights according to the change of loss function value.

3.3 CNN architecture

We compare and test the performance of the proposed CNN model to various modern ConvNets architectures for classification of the insulator image data set. Modern deep CNN architectures such as InceptionV3, MobileNet, VGG16, and ResNet50 are proven to be efficient future extractors for image classification, recognition, and object detection tasks. These networks perform high classification accuracy on large data sets, such as ImageNet. InceptionV3 is a refined version of the Inception deep convolutional architecture. The complexity of the network with 42-layer is similar to other large models such as VGGNet, but it uses factorizing convolutions that reduce the number of parameters (23.9 M) without decreasing the performance of the model. MobileNet is a small deep neural network (DNN) introduced by Google. It operates using depthwise separable convolutions that result in parameter reduction with 4.2 million parameter size. It is suitable for on-device or embedded applications with limited computation power resources. VGG16 architecture composed of 16 layers is an efficient feature extractor with only 3×3 convolutions due to the number of filters applied. However, the network is computationally expensive since it consists of 138 million parameters. ResNet50 is a 50 layer Residual Network architecture composed of several blocks and 23.6 million parameters. Each block performs convolution, batch normalisation, and ReLU activation.

3.3.1 Implementations: The implementation was done with Python Tensorflow and the performance analysis done using image data set processed by a different set of filters, as explained in previous sections. The CNN was constructed using different activation, optimisation and loss functions, having the following neural network system parameters: batch size, 16; epochs, 100, convolutional filter size, $32 \times 2 \times 2$; dropout, 0.5 The database is divided into train and validation sets, containing four classes, and a total of 400 images with 200 for training and 200 images for validation. The proposed CNN architecture consists of an input layer, three hidden layers, which include convolutional layers, pooling, and ReLU activation layers. This is followed by dropout (0.5) to prevent overfitting. The activation functions used are sigmoid, and softmax and the system are tested using two loss functions cross-entropy and mean squared error.

4 Results and discussion

ML classifiers: The ML classifiers identified in Tables 1–4 are used for performing comparisons. Ten-fold cross-validation with 100 iterations is performed for obtaining the results. The mean performance values and its STD is reported. To perform statistical comparisons on STD feature extraction, BN classifier was chosen as the test base. While to compare LBP feature extraction, SMO classifier was set as the test base. In Tables 1–4 '*' indicates that classifier performs statistically worse than the base one (BN or SMO), while '*v*' symbol indicates that the classifier is statistically better than the test base classifier.

The method of classification is multiclass pattern recognition 'one to all'. We have four classes, therefore in a one-to-all problem, we have four binary classification problems. The reason for doing this is for taking into account practical scenario where the objective is to identify the presence or absence of one particular condition. Such a classification system is useful to improve the robustness of classification problem when the test set would have classes which are unknown to the training set.

Table 3 Performance of classifiers: snow on insulator surface

Measure	Processing	BN	NB	SMO	IBK	AdaBoostM1	J48	RF
accuracy, %	STD/mean	**95.40(2.84)**	95.60(3.43)	95.05(3.76)	93.60(3.54)	**96.20(2.85)**	**95.93(2.86)**	**96.10(2.96)**
AUC	STD/mean	**0.98(0.03)**	0.98(0.03)	0.94(0.05) *	0.91(0.05) *	**0.98(0.03)**	**0.94(0.05)***	**0.98(0.03)**
accuracy, %	STD/LMN	89.42(4.83)	89.23(4.72)	81.65(4.48)*	85.85(4.81)	87.77(4.73)	89.60(4.46)	87.00(4.69)
AUC	STD/LMN	0.93(0.03)	0.95(0.03)	0.66(0.09)*	0.81(0.07)*	0.95(0.03) v	0.92(0.04)	0.94(0.03)
accuracy, %	STD/Retinex	88.85(4.37)	88.62(4.28)	89.25(3.93)	85.47(5.08)*	88.82(4.23)	88.20(4.94)	87.30(5.16)
AUC	STD /Retinex	0.89(0.06)	0.93(0.04) v	0.81(0.07)*	0.82(0.07)*	0.91(0.04)	0.85(0.07)	0.91(0.05)
accuracy, %	LBP/mean	75.33(4.56)	70.50(7.04)	74.58(6.40)	75.22(0.72)	71.52(5.88)	68.08(7.28)*	74.97(0.25)
AUC	LBP/mean	0.59(0.07)	0.77(0.07) v	0.71(0.09) v	0.50(0.01)*	0.66(0.10)	0.57(0.10)	0.63(0.10)
accuracy, %	LBP/LMN	75.07(3.44)	69.43(5.11)*	75.10(3.64)	75.00(0.00)	71.77(5.62)	64.45(7.12)*	75.00(0.00)
AUC	LBP/LMN	0.54(0.06)	0.62(0.08)	0.58(0.07)	0.50(0.00)*	0.62(0.11)	0.54(0.11)	0.68(0.08)
accuracy, %	LBP/Retinex	80.42(4.40)	81.00(6.22)	72.18(5.96)*	33.95(5.73)*	73.83(5.44)*	71.97(6.39)*	79.85(3.31)
AUC	LBP/Retinex	0.67(0.07)	0.82(0.08) v	0.69(0.08)	0.53(0.06)*	0.69(0.07)	0.63(0.09)	0.83(0.08) v

Table 4 Performance of classifiers: water droplets on insulator surface

Measure	Processing	BN	NB	SMO	IBK	AdaBoostM1	J48	RF
percent correct	STD/Mean	78.88(3.63)	75.83(5.60)	75.00(0)*	67.27(6.08)*	77.97(4.14)	78.55(3.98)	70.38(6.07)*
AUC	STD/Mean	0.74(0.06)	0.76(0.08)	0.50(0.00)*	0.57(0.08)*	0.73(0.07)	0.58(0.06)*	0.71(0.09)
accuracy, %	STD/LMN	95.60(2.98)	92.10(3.55)*	90.45(3.99)*	95.43(2.93)	96.27(2.76)	95.12(2.60)	95.27(2.93)
AUC	STD/LMN	0.99(0.01)	0.96(0.03)*	0.86(0.06)*	0.94(0.05)*	0.99(0.01)	0.97(0.02)*	0.99(0.01)
accuracy, %	STD/Retinex	74.25(2.45)	76.27(5.26)	75.00(0.00)	72.88(6.37)	73.37(4.53)	74.07(3.58)	75.73(5.58)
AUC	STD /Retinex	0.63(0.06)	0.75(0.09) v	0.50(0.00)*	0.63(0.09)	0.69(0.08) v	0.60(0.09)	0.73(0.10) v
accuracy, %	LBP/mean	**98.73(1.79)**	**99.80(0.68)**	94.55(3.34)*	55.53(11.14)*	94.85(3.64)*	87.65(4.83)*	**97.00(2.82)**
AUC	LBP/Mean	**0.97(0.04)**	**1.00(0.00) v**	0.93(0.06)*	0.70(0.07)*	0.99(0.01)	0.84(0.08)*	**0.99(0.02)**
accuracy, %	LBP/LMN	97.08(2.36)	99.75(0.75) v	86.90(3.73)*	27.82(5.06)*	93.02(4.07)*	90.50(4.75)*	86.98(4.19)*
AUC	LBP/LMN	0.94(0.05)	1.00(0.01) v	0.77(0.08)*	0.52(0.03)*	0.97(0.02)	0.86(0.08)*	1.00(0.00) v
accuracy, %	LBP/Retinex	72.50(3.22)	65.95(6.02)*	61.72(7.50)*	75.00(0.00) v	69.25(6.60)	67.38(6.98)*	75.00(0.00) v
AUC	LBP/Retinex	0.50(0.04)	0.58(0.08)	0.64(0.08) v	0.50(0.01)	0.58(0.11) v	0.57(0.09)	0.73(0.07) v

Table 5 Performance of ML classifiers based on mean filter

ML classifiers	Feature extraction	Accuracy, %
BN	STD/LBP	78 (±18)/83 (±4)
NB	STD/LBP	82 (±3.6)/85 (±4.8)
SMO	STD/LBP	80 (±1.2)/ 86 (±3.5)
IBK	STD/LBP	78 (±5.2)/69 (±2.5)
AB M1	STD/LBP	82 (±4)/79 (±5.4)
J48	STD/LBP	83 (±18.6)/75 (±6)
RF	STD/LBP	80 (±5)/82 (±2)

Table 6 Performance of ML classifiers based on LMN filter

ML classifiers	Feature extraction	Accuracy, %
BN	STD/LBP	90 (±4)/78 (±4)
NB	STD/LBP	78 (±4)/76 (±4)
SMO	STD/LBP	80 (±2)/82 (±3)
IBK	STD/LBP	88 (±5)/63 (±2)
AB M1	STD/LBP	88 (±4)/77 (±5)
J48	STD/LBP	90 (±4)/72 (±6)
RF	STD/LBP	89 (±4)/78 (±1)

Table 7 Performance of ML classifiers based on the retinex filter

ML classifiers	Feature extraction	Accuracy, %
BN	STD/LBP	78 (±2)/73 (±6)
NB	STD/LBP	78 (±4)/68 (±7)
SMO	STD/LBP	78 (±1)/ 78 (±4)
IBK	STD/LBP	76(±4)/66 (±4)
AB M1	STD/LBP	78 (±3)/72 (±6)
J48	STD/LBP	79 (±3)/70 (±6)
RF	STD/LBP	80 (±6)/78 (±3)

The classification accuracy shows the best performance of the classifier and the AUC shows the overall discrimination ability of the classifier. Receiver operating characteristic curve also shows a possible trade-off between accuracy and error rates for a particular class. AUC is defined in terms of the receiver operating characteristic curve and provides a single-value summary (ranging from 0 to 1) for the performance of the learning algorithms.

Table 1 indicates the performance of the ML classifiers when evaluating the detection of insulators clean surfaces. In such a situation since glass insulators are used, they tend to images with large illumination variability. The results show that the combination of STD/LMN feature extraction provides the best performance, which is indicative of the fact that LMN is able to generate illumination invariant features and preserves the edge features from STD feature extraction. The classifiers BN, AB M1, and RF, shows the best results under these conditions.

Tables 2–4 show the performance of the ML classifiers when the insulators are covered with ice, snow, or water droplets. The impact of this is more like a change in the texture of the surface, and that of having pixel noise. The ice and water droplets provide a layer on the surface of the insulator, were often in the early stages, part of the insulator surface is still visible. It is well known in imaging processing studies that LBP is good at discriminating textures, and the results on ice (Tables 2 and 4) are indicative of these. The snow, on the other hand, is opaque and completely changes the texture of the insulator surface, with practically quite often little exposure to the insulator surface. In this case, the snow is more responsive to the STD features as they provide the unique grained surface features of the snow on insulator, and is evident from the relatively better performance of STD/mean combination. The overall performance of the ML algorithms when STD/LBP features are used for mean, LMN, and retinex filters are illustrated in Tables 5–7. It can be seen that in most cases in a multiclass scenario, the STD features outperforms the LBP features irrespective of the combinations of ML algorithm and filters. The filters have the role in normalising the features to make the

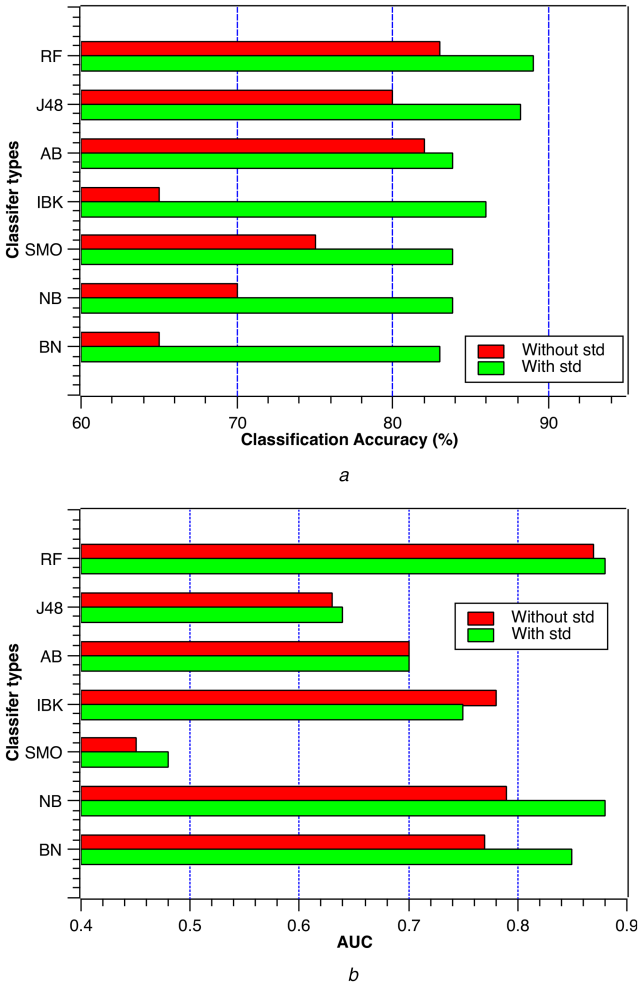

Fig. 7 *Graphs illustrate the impact of Gaussian noise with zero mean and 1% STD on clean insulator images surfaces without and with STD feature extraction. The comparison in*

(a) Shows the classification accuracy, ***(b)*** Shows the AUC values. The classifiers compared are BN, NB, SMO, IBK, AB M1, J48, and RF

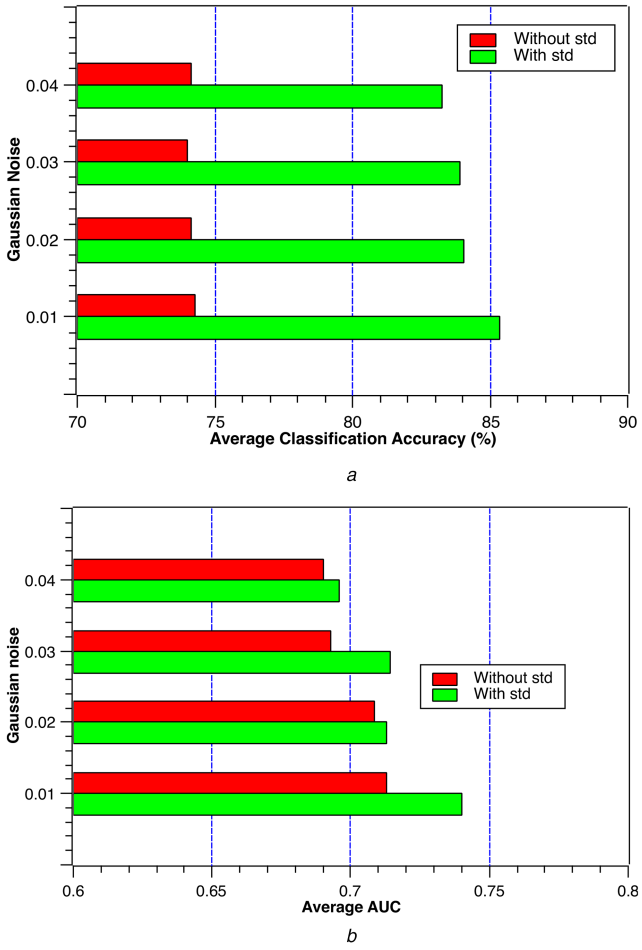

Fig. 8 *Graphs illustrate the impact of Gaussian noise with zero mean and varied STD values (y-axis) on clean insulator images surfaces without and with STD feature extraction. The comparison in*

(a) Shows the average classification accuracy, ***(b)*** Shows the average AUC values across the seven classifiers (i.e. BN, NB, SMO, IBK, AB M1, J48, and RF)

comparisons fair for the classifier. Also, the filters help with reducing the issues with illumination variability.

Noise robustness: The ML algorithms are sensitive to the noise. To test this, we do not apply any feature extraction and instead add Gaussian noise of varying degrees. The Gaussian noise with mean zero and variance of 1%–4% is applied to analyse the sensitivity. In almost all the cases with an increase in the variance, the performance accuracy, and AUC values drop indicating that ML classifiers require feature extraction and normalisation stage. The results of 1% Gaussian noise are reported in Fig. 7, and average performance across different noise levels on the seven classifiers are shown in Fig. 8.

To assess the impact of filtering on the performance robustness of the ML algorithms, we repeat the robustness tests with and without the application of STD features reporting classification accuracy in Fig. 7*a*, and AUC in Fig. 7*b*. The obtained results in Fig. 7 shows that the overall the robustness of the classifiers increased in-terms of classification accuracy and AUC values when STD features are used. The classification accuracy and AUC values overall has improved, making the classifiers less sensitive to the noise. For example, comparison in Fig. 7*a*, the classification accuracy, on average, improved substantially from the range of 74.28–84.65%, which indicates the importance of the feature extraction stage in ML classifiers. The comparison of Fig. 7*b* indicates that on average the AUC values increased from 0.71 to 0.74 with the addition of the feature extraction stage. We also observed this increase across all the different insulator conditions.

The noise robustness is illustrated in Fig. 8. The average performance across seven classifiers [i.e. BN, NB, SMO, IBK, AB M1, J48, and RF] for varied Gaussian noise with STD from 1 to 4% is shown in Fig. 8. Here, Fig. 8*a* shows the average classification accuracy, while Fig. 8*b* shows the average AUC. The application of the noise does not deteriorate the performance improvements shown by feature extraction, and clearly outperforms the case without feature extraction even with the increase in noise levels indicative of the overall robustness of the feature extraction.

CNN classifier:: Tables 8 and 9 illustrate the results of classifying filtered images into one of the four categories achieved by two different loss functions – cross-entropy and mean squared error and activation functions such as softmax and sigmoid. As it can be seen, the accuracy reached only 87% by using softmax and rmsprop functions. This could be due to the limited number of samples and the detection accuracy still has much room for improvement.

NN versus ML classifiers: The major advantage of a DNN classifier is that it does not need intensive hand-coded data preparation and feature extraction. The ML classifiers, on the other hand, requires well-thought-out feature extraction for achieving high classification accuracy. Table 8 and 9 show the limitations of the neural networks, when the data set is small, the accuracy is not as good as ML classifiers shown in Tables 5–7. It is also quite well known that most of the ML classifiers are difficult to be scaled with the increased data set, and their parallel computing implementation complexity is high. The DNN classifiers, on the other hand, consist of dot-product computations as its core computational unit, which is relatively easier to scale with data set increase in parallel processing hardware. To test this hypothesis, we increase the image data set and test the performance of different well-known convolutional neural network algorithms.

Table 8 Averaged CNN classification accuracy based on MSE

Activation/filter	Adam, %	adagrad, %	adadelta, %	adamax, %	rmsprop, %
softmax/mean filter	80	85	73	85	87
softmax/LMN filter	51	68	59	78	77
sotfmax/retinex	29	30	32	33	32
sigmoid/mean	69	87	41	63	85
sigmoid/LMN	81	56	79	73	81
sigmoid/retinex	31	31	36	30	31

Table 9 Averaged CNN classification accuracy using cross entropy loss function

Activation/filter	adam, %	adagrad, %	adadelta, %	adamax, %	rmsprop, %
softmax/mean filter	87	83	72	85	83
softmax/LMN filter	53	75	82	39	87
sotfmax/retinex	32	35	32	30	35
sigmoid/mean	81	81	85	36	81
sigmoid/LMN	53	46	75	47	60
sigmoid/retinex	33	34	33	35	35

Table 10 Comparison of CNN model to state-of-the-art CNN architectures

Architecture	Accuracy, %	Transfer learning accuracy, %	Total trainable parameters
CNN	85	na	70.5 k
inceptionV3	28	56	24.1 M
mobileNetV1	40	41	3.4 M
VGGNet16	34	93	15.4 M
resNet50	25	61	24.1 M

NA, not applicable

Large insulator data set: The image data set is further enhanced with 4000 aerial images of outdoor high voltage glass insulator acquired from a UAV camera. The data set includes four classes with 800 original images and 3200 pre-processed data using different types of noises such as Gaussian, Salt and Pepper, Poisson, and Speckle. The noises are applied to increase the database and take into account possible environmental effects during data acquisition. Images are collected via the drone in the winter conditions. Different states of insulator surface, including snow, ice, and water captured using DJI drone with 20 megapixel CMOS sensor. Each class consists of 1000 images of original and filtered images with a size of 254×103. The data is split by 50% for train and 50% testing stages.

Performance comparison of different DNNs: DNNs based on CNN have two important characteristics: (i) a set of convolutional layers that can learn feature representations, and (ii) an inference network that can be trained to discriminate the classes. In essence, a deep learning network does not require a separate feature extraction stage provided there is sufficient training samples. The selection of hyperparameters of the neural networks is essential to ensure optimal training for a given training data.

The neural networks are data-driven approaches, and the optimisation of hyperparameters are mission critical for its performance improvements. There are several CNN-based architectures today that have different combinations of hyperparameters based on the number of neurons and layers, types of activation functions, and inference scheme adopted. An increase in the number of layers warrants a more extensive training set. In several practical problems, it is not feasible to form large data set as they are usually not fully automated and requires significant investments in data preparation, validation, and verification. Table 10 shows the results when the popular networks such as InceptionV3, MobileNet, VGG16, and ResNet50 are trained using the developed insulator data set. In comparison with the proposed CNN configuration, when using all trainable parameters, these CNNs perform poorly as they are not optimised for this data set. These large CNNs needs larger training data set and is usually useful for a large number of classes with a large number of training samples. In our problem, at present, we do not have a large number of classes, nor there is a need to have a large data set, and for this reason, a smaller optimized CNN will be sufficient to achieve reliable accuracy. The strategies such as transfer learning can be applied to improve the classification accuracy of the state of the art CNN architectures, which are proven to have high classification accuracy once trained on large data set such as imageNet. The convolutional layers can use pre-trained weights that were trained using a large data set, and the inference layer weights can be fine-tuned to fit into the smaller data set. Transfer learning can reduce the number of epochs required to training the network; however, it still does not negate the need to have an even larger data set for achieving high performance and robustness. For example, the InceptionV3 when using the pre-trained network and transfer learning with 50 epochs (same number of the epoch as that of the simple CNN) gives 57% classification accuracy, which is an increase from 28% when training InceptionV3 using all trainable parameters. This indicates that a more substantial number of epochs and more extensive training data is essential to optimise larger CNNs.

5 Conclusion

The images of glass insulator surface under clean, snow, ice, and wet conditions are investigated by using the state of the art image classification techniques. The performance of different ML algorithms is tested and compared based on normalisation filters such as LMN, retinex, and mean and statistical and LBP features. The filters are applied before processing to reduce noise and illumination influence. LBP and statistical features are utilised to extract the textural information for the further classification process. The recognition accuracy of four class patterns was analysed. Application of Bayes Naive, BN, and RF gives the most promising results. The performance of CNN also was tested on the same database. Although the outcome of the network was below compared to other classifiers, it can be improved by enlarging the sise of data and adjusting the layers of the network.

The data set sample size was increase and tested on simple CNN to larger well known CNN algorithms such as InceptionV3, MobileNetV1, VGGNet16, and ResNet50. The simplistic CNN showed excellent performance in comparison with the state of the art while utilizing a significantly smaller number of trainable parameters. Overall, the proposed method could be implemented for a real-time condition assessment of outdoor insulator surface. In future work for the evaluation of the insulator state integration of additional information, such as leakage current, to image-based monitoring process would be beneficial.

6 Acknowledgments

We thank the anonymous reviewers, Guest Editor, and the Editor-in-Chief for their valuable suggestions that helped to improve the quality of the work.

7 References

[1] Zhang, Z., Wei, D., Zhang, D., *et al.*: 'Effects of ring-shaped non-uniform pollution on outdoor insulation electrical property', *IEEE Trans. Dielectr. Electr. Insul.*, 2017, **24**, (6), pp. 3603–3611

[2] Burnham, J.T., Waidelich, R.J.: 'Gunshot damage to ceramic and nonceramic insulators', *IEEE Trans. Power Deliv.*, 1997, **12**, (4), pp. 1651–1656

[3] Prasad, D.S., Reddy, B.S.: 'Impact of mist and acidic fog on polymer insulator samples exposed to corona discharges', *IEEE Trans. Dielectr. Electr. Insul.*, 2016, **23**, (3), pp. 1546–1554

[4] Venkataraman, S., Gorur, R.S., Mishra, A.P.: 'Impact of weathering on flashover performance of nonceramic insulators', *IEEE Trans. Dielectr. Electr. Insul.*, 2008, **15**, (4), pp. 1073–1080

[5] Song, W., Shen, W.-W., Zhang, G.-J., *et al.*: 'Aging characterization of high temperature vulcanized silicone rubber housing material used for outdoor insulation', *IEEE Trans. Dielectr. Electr. Insul.*, 2015, **22**, (2), pp. 961–969

[6] Nazir, M.T., Phung, B.T., Yu, S., *et al.*: 'Tracking, erosion and thermal distribution of micro-aln + nano-sio2 co-filled silicone rubber for high-voltage outdoor insulation', *High Voltage*, 2018, **3**, (4), pp. 289–294

[7] Momen, G., Farzaneh, M., Nekahi, A., *et al.*: 'Properties and applications of superhydrophobic coatings in high voltage outdoor insulation: a review', *IEEE Trans. Dielectr. Electr. Insul.*, 2017, **24**, (6), pp. 3630–3646

[8] Zhang, X., Rowland, S.M.: 'Stability and energy of low current surface discharges on wet surfaces', *IEEE Trans. Dielectr. Electr. Insul.*, 2012, **19**, (6), pp. 2055–2062

[9] Cao, B., Wang, L., Li, X., *et al.*: 'Influence of partial electric arc on the contamination degree monitoring system in view of leakage current', *IEEE Trans. Dielectr. Electr. Insul.*, 2018, **25**, (4), pp. 1545–1552

[10] Pylarinos, D., Siderakis, K., Thalassinakis, E.: 'Comparative investigation of silicone rubber composite and room temperature vulcanized coated glass insulators installed in coastal overhead transmission lines', *IEEE Electr. Insul. Mag.*, 2015, **31**, (2), pp. 23–29

[11] Liu, Y., Farzaneh, M., Du, B.X.: 'Nonlinear characteristics of leakage current for flashover monitoring of ice-covered suspension insulators', *IEEE Trans. Dielectr. Electr. Insul.*, 2016, **23**, (3), pp. 1242–1250

[12] Li, H., Qiao, Q.: 'Localisation of insulator strings' images based on colour filtering and texture matching', *J Eng.*, 2019, **2019**, (16), pp. 2790–2793

[13] Zhai, Y., Chen, R., Yang, Q., *et al.*: 'Insulator fault detection based on spatial morphological features of aerial images', *IEEE. Access.*, 2018, **6**, pp. 35316–35326

[14] Pernebayeva, D., Sadykova, D., MBagheri, J.A.P.: 'Outdoor insulator surface condition evaluation using image classification'. 2018 IEEE Int. Conf. High Voltage Engineering and Application (ICHVE), Athens, Greece, 2018, pp. 1–4

[15] McCann, J.: 'Retinex theory'. Encyclopedia of Color Science and Technology, New York, NY, USA, 2016, pp. 1118–1125

[16] Gao, Y., Hu, H.-M., Li, B., *et al.*: 'Naturalness preserved nonuniform illumination estimation for image enhancement based on retinex', *IEEE Trans. Multimedia*, 2018, **20**, (2), pp. 335–344

[17] James, A.P., Dimitrijev, S.: 'Inter-image outliers and their application to image classification', *Pattern Recognit.*, 2010, **43**, (12), pp. 4101–4112

[18] Guo, Z., Zhang, L., Zhang, D.: 'A completed modeling of local binary pattern operator for texture classification', *IEEE Trans. Image Process.*, 2010, **19**, (6), pp. 1657–1663

[19] Ojala, T., Pietikäinen, M., Mäenpää, T.: 'Multiresolution gray-scale and rotation invariant texture classification with local binary patterns', *IEEE Trans. Pattern Anal Mach. Intell.*, 2002, **24**, (7), pp. 971–987

[20] Friedman, N., Geiger, D., Goldszmidt, M.: 'Bayesian network classifiers', *Mach. Learning*, 1997, **29**, (2-3), pp. 131–163

[21] Nookala, G.K.M., Pottumuthu, B.K., Orsu, N., *et al.*: 'Performance analysis and evaluation of different data mining algorithms used for cancer classification', *Int. J. Adv. Res. Artif. Intell.*, 2013, **2**, (5), pp. 49–55

[22] López, J., Suykens, J.AK.: 'First and second order SMO algorithms for ls-SVM classifiers', *Neural Process. Lett.*, 2011, **33**, (1), pp. 31–44

[23] Choudhury, S., Bhowal, A.: 'Comparative analysis of machine learning algorithms along with classifiers for network intrusion detection'. 2015 Int. Conf. on Smart Technologies and Management for Computing, Communication, Controls, Energy and Materials (ICSTM), Chennai, India, 2015, pp. 89–95

[24] Wang, J., Xiong, X., Zhou, N., *et al.*: 'Early warning method for transmission line galloping based on SVM and adaboost bi-level classifiers', *IET Gener. Transm. Distrib.*, 2016, **10**, (14), pp. 3499–3507

[25] Shin, H.-C., Roth, H.R., Gao, M., *et al.*: 'Deep convolutional neural networks for computer-aided detection: CNN architectures, dataset characteristics and transfer learning', *IEEE Trans. Med. Imaging*, 2016, **35**, (5), pp. 1285–1298

[26] Song, L., Liu, J., Qian, B., *et al.*: 'A deep multi-modal CNN for multi-instance multi-label image classification', *IEEE Trans. Image Process.*, 2018, **27**, (12), pp. 6025–6038

[27] Zhao, Z., Fan, X., Xu, G., *et al.*: 'Aggregating deep convolutional feature maps for insulator detection in infrared images', *IEEE. Access.*, 2017, **5**, pp. 21831–21839

[28] Lei, X., Sui, Z.: 'Intelligent fault detection of high voltage line based on the faster R-CNN', *Measurement*, 2019, **138**, pp. 379–385

[29] Liu, Y., Pei, S., Fu, W., *et al.*: 'The discrimination method as applied to a deteriorated porcelain insulator used in transmission lines on the basis of a convolution neural network', *IEEE Trans. Dielectr. Electr. Insul.*, 2017, **24**, (6), pp. 3559–3566